Max-Planck-Institut für Meteorologie

REPORT No. 61

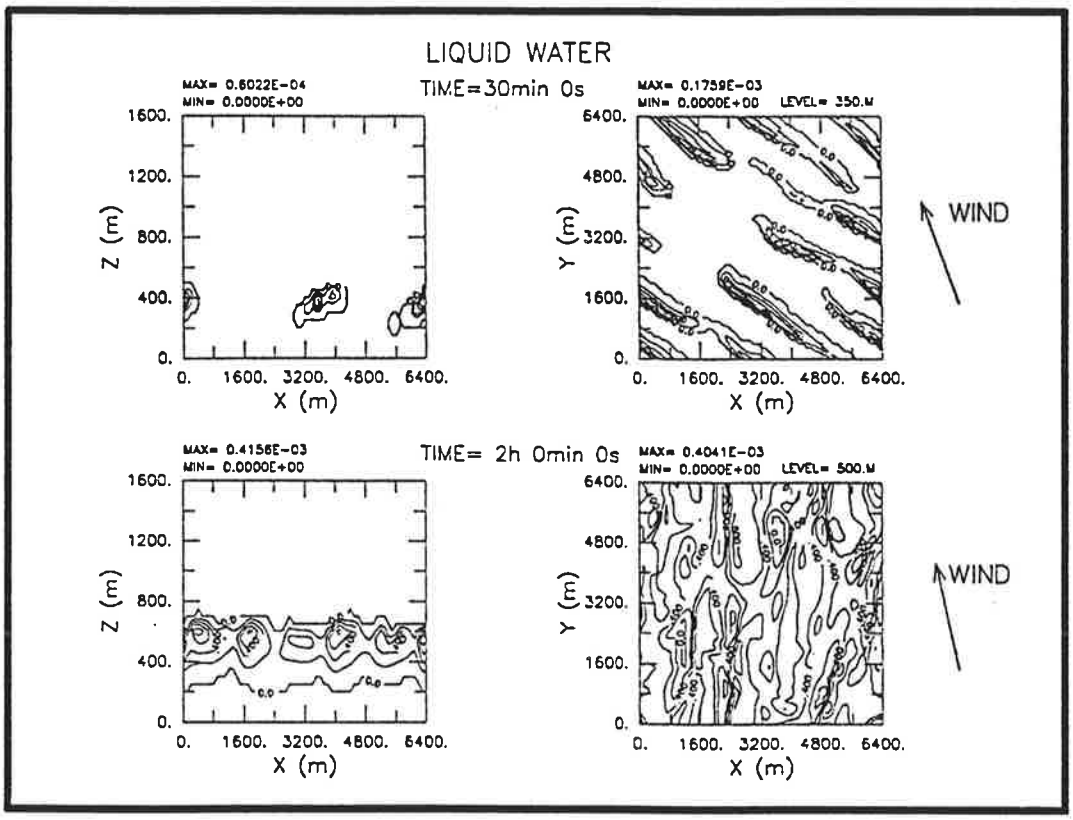

THREE-DIMENSIONAL SIMULATION OF CLOUD STREET DEVELOPMENT DURING A COLD AIR OUTBREAK

by

ANDREAS CHLOND

HAMBURG, MARCH 1991

AUTHOR:

ANDREAS CHLOND

MAX-PLANCK-INSTITUT
FUER METEOROLOGIE

SUBMITTED TO
BOUNDARY-LAYER METEOROLOGY

MAX-PLANCK-INSTITUT
FUER METEOROLOGIE
BUNDESSTRASSE 55
D-2000 HAMBURG 13
F.R. GERMANY

Tel.: (040) 4 11 73-0
Telex: 211092 mpime d
Telemail: MPI.METEOROLOGY
Telefax: (040) 4 11 73-298

REPb 61

Three-Dimensional Simulation of Cloud Street Development during a Cold Air Outbreak

A. Chlond

Max-Planck-Institut für Meteorologie
Hamburg, FRG

ISSN 0937–1060

Abstract

A three-dimensional numerical model is used to study the boundary-layer eddy structure under conditions during a cold air outbreak. The model explicitly represents the large-scale three-dimensional motions, while the small-scale turbulence is parameterized; it contains a water cycle with cloud formation and it takes into account infrared radiative cooling in cloudy conditions and the influence of large-scale vertical motions.

The model is applied to conditions corresponding to an observed case of cloud street/stratocumulus development which occurred over the Greenland Sea during the 1988 ARKTIS experiment. The boundary layer is found to grow rapidly as the cold air flows off the ice over the relatively warm water. Coherent structures were identified in this boundary layer. It is found that the rolls become increasingly more convective in character with distance from the ice edge. Qualitative and quantitative descriptions of the flow field are given. Additionaly, the relative importance of the various physical processes and external parameters in the evolution of the mean field of variables is indicated.

1. *Introduction*

Areas of convective activity are usually associated with the flow of cold air over warm water, such as in cold air outbreaks in mid-latitudes. In such a case northerly winds bring cold and dry polar air masses from the interior of the continent and the ice pack south over the relatively warm open waters of the ocean. Cloud streets are formed 100 km or less downstream from the coast line and simply provide flow visualization of the flow patterns developing within the convective boundary layer. The conception is that the secondary flow consists of horizontal roll vortices which extend throughout the depth of the boundary layer. Their axis is roughly in the direction of the basic flow and parallel stripes of upward motion within these helical motions may in some cases be marked with clouds. In other cases, the rolls are indicated by rows of dense dark clouds within a solid cloud cover. The spacing between adjacent cloud lines is normally between 2 and 8 km and they persist for several hundred kilometers south of the ice edge where a transformation takes place to a three-dimensional cellular convective regime.

The conditions for the formation of these rolls have been the subject of many theoretical and observational studies, e.g. Küttner (1971), Le Mone (1973) and Brown (1980). The cause of the rolls has been attributed to both a shear instability of the Ekman planetary boundary layer and the organization of buoyant convection by velocity shear. Often it is a combination of these two instability mechanisms. A number of observational studies of cloud street formation during cold air outbreaks (Walter, 1980; Miura, 1986) have provided information as to how the interval between the cloud lines changes with distance south of the edge of the ice pack, but not on turbulent and roll-scale transports of momentum and energy. Therefore, it might be useful to apply a numerical model to the cold air outbreak problem, with special emphasis on the boundary layer eddy structure and on turbulent statistics.

The observed two-dimensionality has formed the basis for several numerical studies, e.g. Mason and Sykes (1982), Mason (1985), Etling and Raasch (1987), Chlond (1987), Sykes et al. (1988, 1990), and Raasch (1990). These studies have provided a better understanding of the physical processes involved, and have given a detailed information on roll-scale velocity variances and roll-scale vertical transports. However, since the models used have assumed homogeneous conditions in the direction of the roll axis, they cannot predict whether two-dimensional eddies should actually dominate the flow. In addition,

calculations by Chlond (1987) lead to the suggestion that the relation between the cross-roll and along-roll velocity variances cannot be reproduced in the right manner by two-dimensional models.

Therefore, we try to extend this work. Unlike previous studies of the moist convective boundary layer, which were subject to limitations in the ability to resolve the actual eddy structure, our primary interest here is in simulating the temporal development of three-dimensional boundary layer flows during cold air outbreaks under conditions where the surface heat flux, latent heat release and radiative fluxes should have a strong effect. Hence, a three-dimensional numerical model has been developed in order to fully take into account circulations acting in both horizontal and the vertical plane. The general idea underlying the model is that of a large-eddy model. The model explicitly calculates the spatial averages, which hopefully represent the dominant large-scale motions, while parameterizing the effect of the fluctuations on the averaged flow quantities. The model includes most of the physical processes occurring in a moist boundary layer in the absence of precipitation. It contains a water cycle with cloud formation (including a subgrid-scale condensation scheme), a treatment of the subgrid scale turbulence which incorporates effects of thermal stratification; it takes into account infrared radiative cooling in cloudy conditions (using an effective emissivity model) and the influence of large-scale vertical motions. The model is applied to conditions corresponding to an observed case of cloud street/stratocumulus development which occurred over the Greenland Sea during the 1988 ARKTIS experiment (Brümmer, 1991). Our principal objectives are to determine the respective roles of condensation, cloud top radiative cooling, large-scale subsidence, the large-scale moisture field and time dependent surface heating on the boundary layer rolls by considering simulations with and without these effects. Although the model is far from being perfect for the simulation of such complex boundary layer phenomena, it can give at least some insight into the exchange process between ocean and atmosphere due to organized vortices in the boundary layer.

The paper proceeds as follows. Section 2 describes the numerical model. This includes the presentation of the basic set of equations, the treatment of the subgrid eddies, the description of the physical processes (e.g. condensation cycle and radiation scheme) and finally, an outline of the numerical methods. Section 3 presents results obtained with a series of 3 h simulations for conditions commonly observed during cold air outbreaks. We will report on the information the model yields concerning the influence of the various physical

$$K_H = S_H \bullet \Lambda \bullet (2\bar{e})^{1/2} \tag{18b}$$

where S_M and S_H are stability-dependent coefficients, similar to those of Mellor and Yamada (1974). Here S_H and S_M are given algebraically by

$$S_H = \frac{(1 - 2b)/3}{A + R_i (2 + 1/(bs))} \tag{19a}$$

$$S_M = \frac{(A^2 + (A/(bs) - 1) R_i}{A + R_i} \cdot S_H \quad , \tag{19b}$$

where the turbulent Richardson number is defined by

$$R_i = \frac{g}{\Theta_\infty} \left(K_1 \frac{\partial \bar{\Theta}}{\partial z} + K_2 \frac{\partial \bar{q}}{\partial z} \right) \frac{\Lambda^2}{2\bar{e}} \quad . \tag{20}$$

The constants in Equation (19) are entirely empirical (Lewellen, 1977). Here we use the values A = 1, s = 1.8 and as already specified b = 0.125.

The length scale Λ is given by

$$\Lambda = \min \left(0.67 \bullet z \ , \ \Delta, \ (2\bar{e}^{1/2}) / N \right) \quad . \tag{21}$$

Here Δ is the average grid scale $\Delta = 1/3\ (\Delta x + \Delta y + \Delta z)$ where Δx, Δy, is Δz are the respective grid intervals and N is the Brunt-Vaisälä frequency, defined by

$$N^2 = \frac{g}{\Theta_\infty} \left(K_1 \frac{\partial \bar{\Theta}}{\partial z} + K_2 \frac{\partial \bar{q}}{\partial z} \right) \quad . \tag{22}$$

Hence, Λ is proportional to z near the surface, but is limited to the average mesh spacing. The third limit is applied only in stable regions where $N^2 > 0$.

The liquid water content is calculated using the formulation of Sommeria and Deardorff (1977). This formulation by-passes the shortcomings of previous condensation schemes which assume that a computational grid volume is either entirely saturated or entirely unsaturated.

This is achived by making allowance for statistical variations of Θ_l and q on the subgrid-scale. In this way local condensation can occur in the presence of large turbulent fluctuations, even though the average state is below saturation. To derive the dependencies of mean cloud fraction and mean liquid water content upon temperature and humidity statistics, it is assumed that the instant value of the quantity $\Delta q = q - q_s(T_l)$ (saturation deficit) is distributed around its grid volume mean value according to a Gaussian probability density function with standard deviation

$$\sigma = \left(\overline{q'^2} - 2\left(\frac{T}{\Theta}\right) \alpha \, \overline{q' \Theta'_l} + \left(\frac{T}{\Theta}\right)^2 \alpha^2 \, \overline{\Theta'^2_l} \right)^{1/2} , \qquad (23)$$

where $\overline{q'^2}$, $\overline{\Theta'^2_l}$ and $\overline{q' \Theta'_l}$ are the variances of q and Θ_l and their covariance which are calculated diagnostically from the subgrid fluxes of q and Θ_l (see below). The mean liquid water content $\overline{q_l}$ and the fraction of grid volume r in which it is contained is then calculated by integration over every possible saturation deficit contributing to liquid water, using that probability density function. Following the usual approximations (Sommeria and Deardorff, 1977), we have

$$\frac{\overline{q_l}}{\gamma \cdot \sigma} = \begin{cases} 0 & Q \le -1.6 \\ \{(Q + 1.6)^2 / 6.4 & |Q| < 1.6 \\ Q & Q \ge 1.6 \end{cases} \qquad (24a)$$

$$r = 0.5\,(1 + Q/1.6) \quad 0 \le r \le 1 \qquad (24b)$$

where $\gamma = (1 + L/c_p \, \alpha)^{-1}$ and Q is a normalized departure from mean saturation

$$Q = \frac{\left(\overline{q} - q_s(\overline{T_l})\right)}{\sigma} . \qquad (25)$$

The standard deviation σ of the saturation deficit will be needed in this calculation. Instead of solving prognostic equations for the variances of q and Θ_l and their covariance a simple diagnostic estimate (but which should have the correct magnitude) of these quantities, according to

$$\overline{q'^2} = \left(\frac{2}{3}\bar{e}\right)^{-1} \sum_{i=1}^{3} \left(\overline{q' u'_i}\right)^2 \tag{26a}$$

$$\overline{\Theta'^2_l} = \left(\frac{2}{3}\bar{e}\right)^{-1} \cdot \sum_{i=1}^{3} \left(\overline{\Theta'_l u'_i}\right)^2 \tag{26b}$$

$$\overline{\Theta'_l q'} = \left(\frac{2}{3}\bar{e}\right)^{-1} \cdot \sum_{i=1}^{3} \overline{q' u'_i} \cdot \overline{\Theta'_l u'_i} \tag{26c}$$

was employed.

2.3. *Boundary and initial conditions*

The computational domain extends horizontally and vertically over a finite domain of size $L_x \cdot L_y \cdot L_z$ (where $L_x = L_y = 6400$ m and $L_z = 1600$ m are used for all runs). At the lateral boundaries, periodicity is assumed. At the top, a zero slope condition on all variables, except $\overline{w}$, $\overline{q}$ and $\overline{\Theta_l}$, is imposed. Vertical velocity $\overline{w}$ is zero at the top and the gradients of $\overline{q}$ and $\overline{\Theta_l}$ are fixed at the initial gradients Γ_q and $\Gamma_{\Theta l}$, respectively. The upper boundary conditions do not allow the transmission of gravity waves which can be generated in a stable layer. This could lead to reflections and to an unrealistic distribution of momentum and energy. To avoid reflections from the top lid, a Rayleigh friction term is added to Equation (5) and (6). In this way, a radiation condition is simulated by an artificial sponge layer in the upper third of the model domain. The coefficient of Rayleigh damping ν is gradually increased in the spong layer according to the square of a sine function.

That is

$$\nu = \nu_o \cdot \sin^2\left(\frac{\pi}{2}(z - z_s)/(L_z - z_s)\right) \quad , \tag{27}$$

where z_s is the base of the sponge layer and $\nu_0 = (300s)^{-1}$.

At the lower boundary, we use Monin-Obukhov similarity to relate the fluxes of various quantities to the corresponding difference between the surface value and the value at the first model grid point above the surface at $z = z_1$. Using the scaling parameters u_*, Θ_* and q_* we obtain the relations

$$\left(\tau_{13}^2 + \tau_{23}^2\right)^{1/2} = u_*^2 \tag{28a}$$

$$H_3 = - u_* \cdot \Theta_* \tag{28b}$$

$$Q_3 = - u_* q_* \tag{28c}$$

The scaling parameters are related to mean field variables through the following,

$$u_* = \frac{\kappa \left(\overline{u}^2 (z_1) + \overline{v}^2(z_1)\right)^{1/2}}{\ln z_1 / z_o - \Psi_M (z_1 / L)} \tag{29a}$$

$$\Theta_* = \frac{\kappa \left(\overline{\Theta_l} (z_1) - \overline{\Theta_l} (z_T)\right)}{\ln z_1 / z_T - \Psi_H (z_1 / z_T)} \quad . \tag{29b}$$

A similar relation to (29b) for q_* can be written, with $\overline{\Theta_l}\,(z_1) - \overline{\Theta_l}\,(z_T)$ replaced by $\overline{q}(z_1) - \overline{q}(z_T)$. In the above, κ is von Karman's constant, z_o and z_T are aerodynamic roughness and temperature surface scaling heights, respectively, and L is the Monin-Obukhov stability length defined by

$$L = \frac{u_*^2}{\kappa \left(g / \Theta_\infty\right)\left(\Theta_* + 0.61 \bullet \Theta_\infty q_*\right)} \tag{30}$$

The ψ functions in Equation (29) can be related to gradient stability functions by

$$\Psi = \int \left(1 - \Phi\,(z/L)\right) d\,(\ln z/L) \,. \tag{31}$$

For $z/L \leq 0$ the Φ functions take the form

$$\Phi_M = \left(1 - \gamma_1 z/L\right)^{-1/4} \tag{32a}$$

$$\Phi_H = \left(1 - \gamma_2 z/L\right)^{-1/2} \quad , \tag{32b}$$

where we choose $\gamma_1 = 20.3$ and $\gamma_2 = 12.2$ according to the recommendations of Webb (1982). In addition $\kappa = 0.4$ is used. Since we are interested in the marine boundary layer in particular, the liquid water potential temperature at the

surface was assumed to be horizontally homogeneous but a prescribed function of time; $\overline{q}$ ($z = z_T$) is set equal to the saturation value at the ocean surface. Finally, zero slope conditions are applied for $\overline{e}$ and $\overline{p}$ at the surface.

The initialization of each run proceeds in the following manner. The initial $\overline{\Theta}_l$-profile is specified by a prescribed temperature difference $\Delta\overline{\Theta}_l$ between the ocean surface and the overlying air and a constant gradient $\Gamma_{\Theta l}$ above. Likewise, the initial humidity profile is specified by a humidity jump $\Delta\overline{q}_l$ and a constant gradient $\Gamma_{\Theta l}$ above. With these values, the initial windprofile is obtained by running a one-dimensional version of the model to steady state. During this phase, temperature and humidity profiles are fixed. In order to drive the system this horizontally homogeneous solution is then transferred to the three-dimensional domain and perturbed by imposing small random perturbations on the temperature field at the first time step.

2.4. Numerical techniques

The numerical integration scheme is based on an equidistant staggered grid and finite difference approximations. All scalars are defined at the cell centres, $\overline{u}$ is evaluated at the middle of the upstream and downstream faces, $\overline{v}$ at the middle of the two cross-stream faces and $\overline{w}$ at the middle of the bottom and top faces. For the advection of SGS-kinetic energy we choose the upstream scheme because it guarantees that positive scalars stay positive. Otherwise, spatial differentials are approximated by second-order accurate central differences in a form which conserves the integral of linear and quadratic quantities up to very small errors (e.g. Piacsek and Williams, 1970; Williams, 1969). Euler time differencing is used in the equation for the SGS kinetic energy; in the balance equations for temperature and humidity time integration is performed using the Adams-Bashforth scheme. The momentum equations are solved by using a predictor-corrector scheme which casts Equations (2) to (4) into

$$\overline{u}_i^{(N+1)^*} = \overline{u}_i^N + \Delta t\left(\frac{3}{2}R_i^N - \frac{1}{2}R_i^{N-1} - \frac{1}{\rho_o}\frac{\partial\overline{p}^N}{\partial x_i}\right) \tag{33a}$$

$$\overline{u}_i^{(N+1)} = \overline{u}_i^{(N+1)^*} - \Delta t\frac{1}{\rho_o}\frac{\partial\Delta p}{\partial x_i}\quad , \tag{33b}$$

where R_i denotes the right-hand sides of Equations (2) to (4) except the pressure gradients and

$$\Delta p = \bar{p}^{N+1} - \bar{p}^{N} \quad . \tag{34}$$

The incompressibility condition requires the implicit determination of pressure, so that the velocity field resulting from Equation (33b) has to satisfy Equation (1). Applying the divergence operator on Equation (33b) yields a Poisson equation for the pressure increment

$$\frac{\partial^2 \Delta p}{\partial x_i \partial x_i} = \frac{\rho_o}{\Delta t} \frac{\partial \bar{u}_i^{(N+1)^*}}{\partial x_i} \quad . \tag{35}$$

This equation is solved by succesive over-relaxation using RED/BLACK decomposition to guarantee vectorization. In this manner the continuity equation is strictly enforced. For the runs presented here, the model domain extends to a height of 1600 m and the length treated in the horizontal directions is 6400 m. The region is split into 64 grid intervals in x, 64 along y and 34 along the vertical z-direction (i.e. $\Delta x = \Delta y = 100$ m, $\Delta z = 50$ m). A time step of $\Delta t = 3$ s was used for all runs. Each simulation hour required about one computer hour on the CRAY-2S computer.

3. *Results*

3.1. *Cases treated*

A series of simulations was carried out in order to demonstrate the models ability to serve as a tool to interpret experimental data and to understand the various physical processes acting in a cloudy convective boundary layer during a cold air outbreak.

Firstly, the model is applied to conditions corresponding to an observed case of cloud street / stratocumulus development which occurred over the Greenland Sea during the 1988 ARKTIS experiment. The experiment took place in the Fram Strait in the area straddling the ice margin west of Spitsbergen during the period from 4 to 26 May 1988. The experiment was dedicated to the study of boundary layer modification and certain cloud structures in cases of off-ice and on-ice air flows.

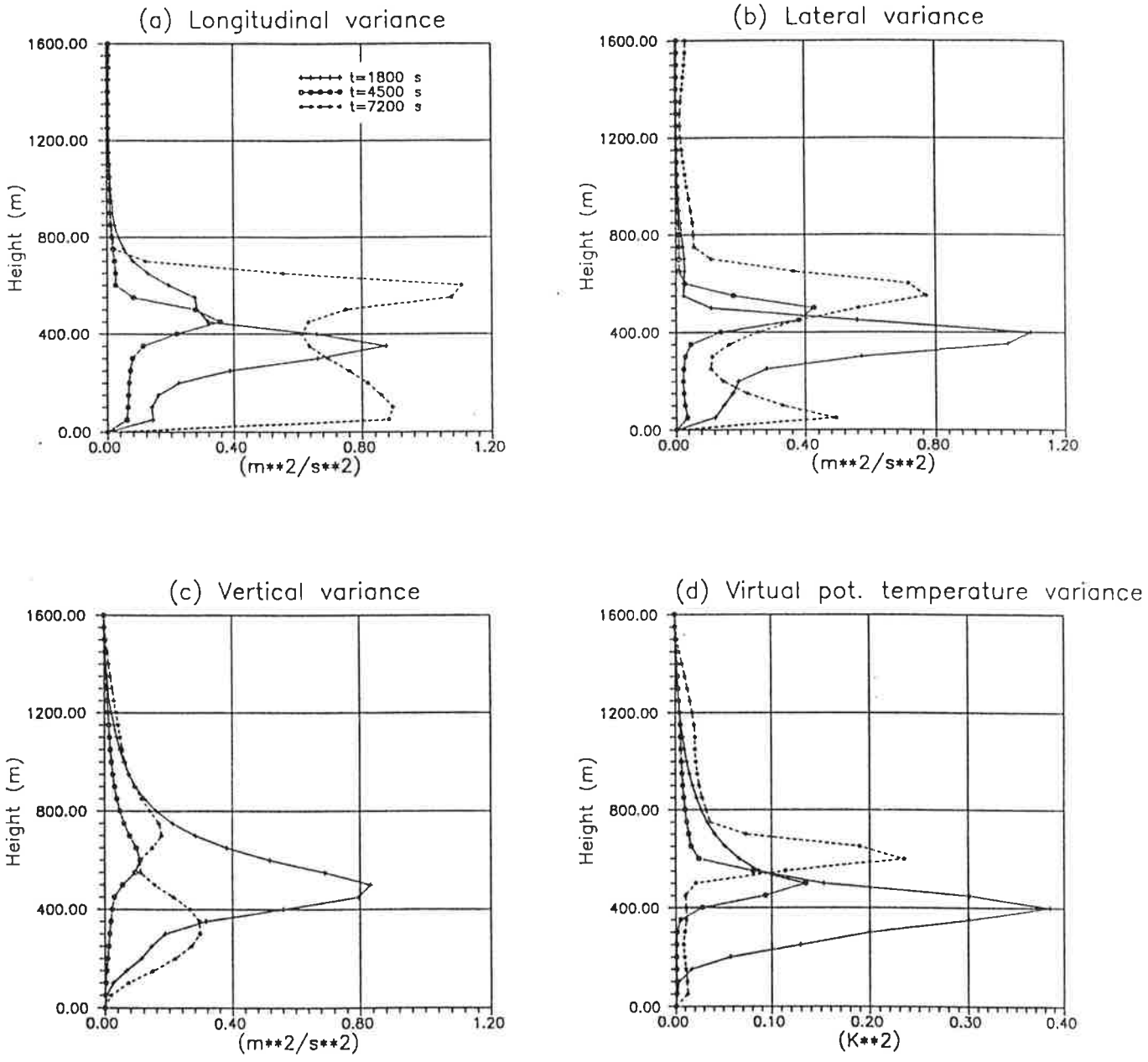
(a) Longitudinal variance
t=1800 s
t=4500 s
t=7200 s
Height (m)
1600.00
1200.00
800.00
400.00
0.00
0.00
0.40
0.80
1.20
(m**2/s**2)
(b) Lateral variance
Height (m)
1600.00
1200.00
800.00
400.00
0.00
0.00
0.40
0.80
1.20
(m**2/s**2)
(c) Vertical variance
Height (m)
1600.00
1200.00
800.00
400.00
0.00
0.00
0.40
0.80
1.20
(m**2/s**2)
(d) Virtual pot. temperature variance
Height (m)
1600.00
1200.00
800.00
400.00
0.00
0.00
0.10
0.20
0.30
0.40
(K**2)

Fig. 6

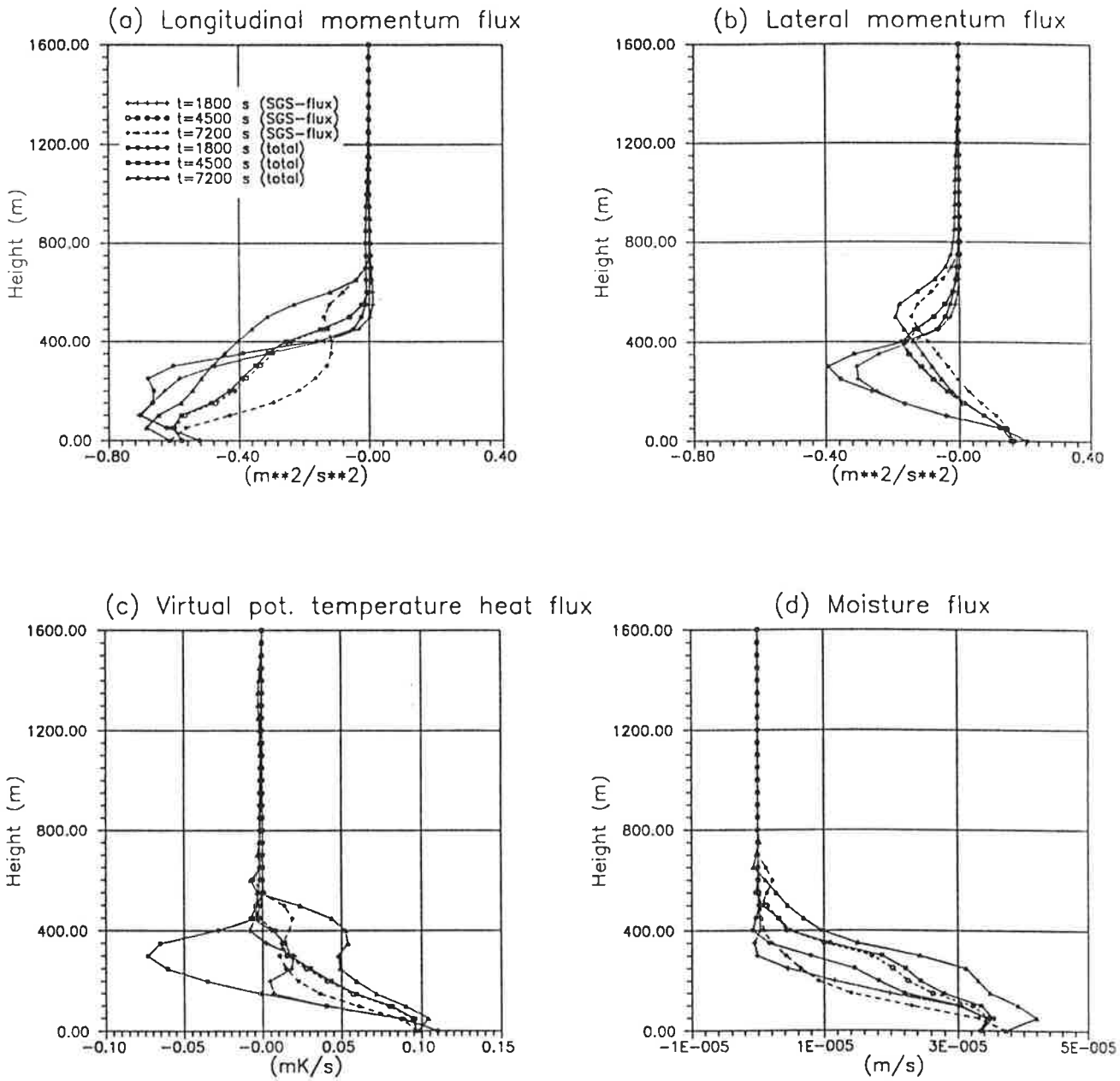
(a) Longitudinal momentum flux
t=1800 s (SGS-flux)
t=4500 s (SGS-flux)
t=7200 s (SGS-flux)
t=1800 s (total)
t=4500 s (total)
t=7200 s (total)
Height (m)
1600.00
1200.00
800.00
400.00
0.00
-0.80
-0.40
-0.00
0.40
(m**2/s**2)
(b) Lateral momentum flux
Height (m)
1600.00
1200.00
800.00
400.00
0.00
-0.80
-0.40
-0.00
0.40
(m**2/s**2)
(c) Virtual pot. temperature heat flux
Height (m)
1600.00
1200.00
800.00
400.00
0.00
-0.10
-0.05
-0.00
0.05
0.10
0.15
(mK/s)
(d) Moisture flux
Height (m)
1600.00
1200.00
800.00
400.00
0.00
-1E-005
1E-005
3E-005
5E-005
(m/s)

Fig. 7

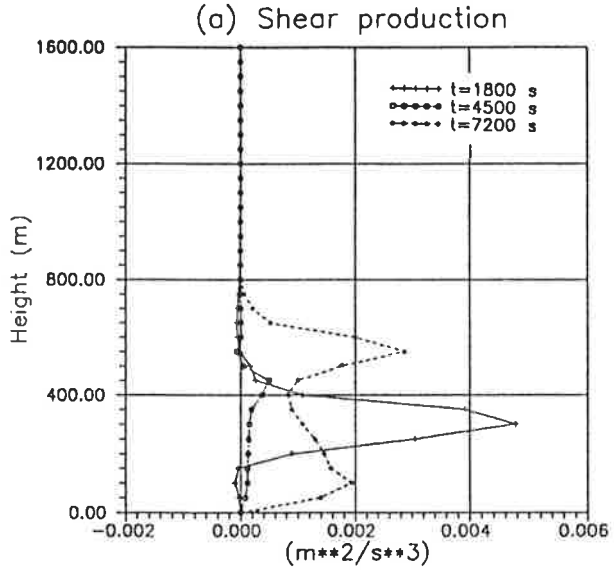
(a) Shear production
1600.00
1200.00
800.00
400.00
0.00
Height (m)
t=1800 s
t=4500 s
t=7200 s
−0.002
0.000
0.002
0.004
0.006
(m**2/s**3)

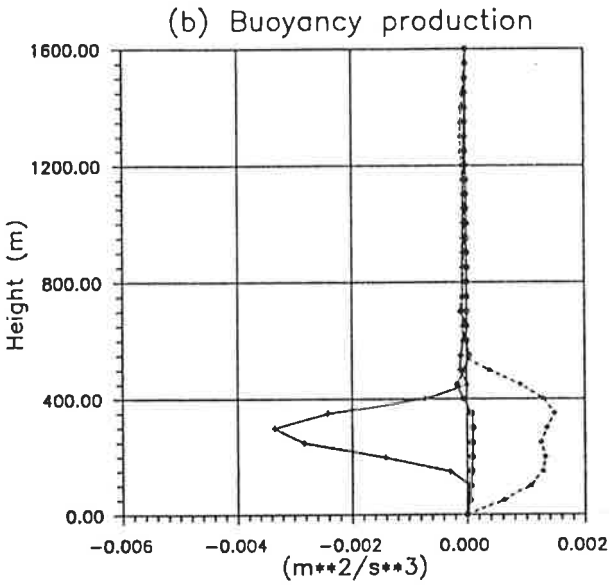
(b) Buoyancy production
1600.00
1200.00
800.00
400.00
0.00
Height (m)
−0.006
−0.004
−0.002
0.000
0.002
(m**2/s**3)

Fig. 8

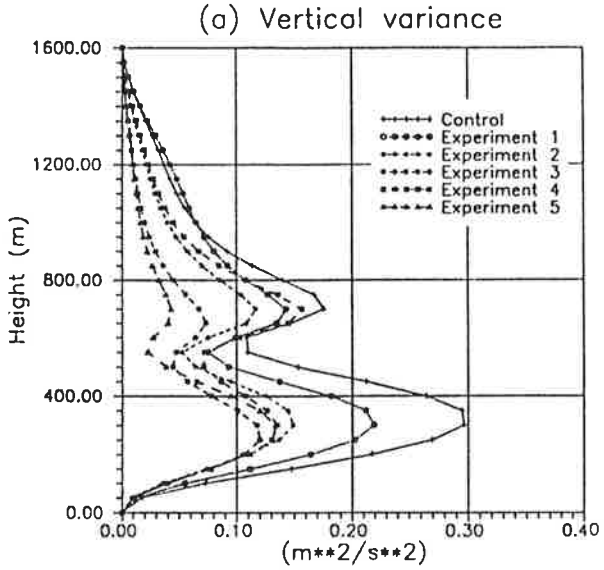
(a) Vertical variance
Control
Experiment 1
Experiment 2
Experiment 3
Experiment 4
Experiment 5
Height (m)
1600.00
1200.00
800.00
400.00
0.00
0.00
0.10
0.20
0.30
0.40
(m**2/s**2)

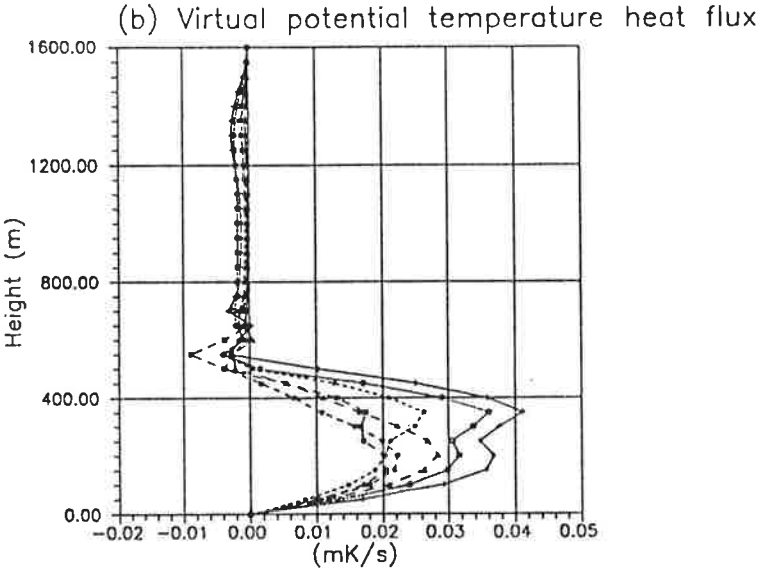
(b) Virtual potential temperature heat flux
Height (m)
1600.00
1200.00
800.00
400.00
0.00
-0.02
-0.01
0.00
0.01
0.02
0.03
0.04
0.05
(mK/s)

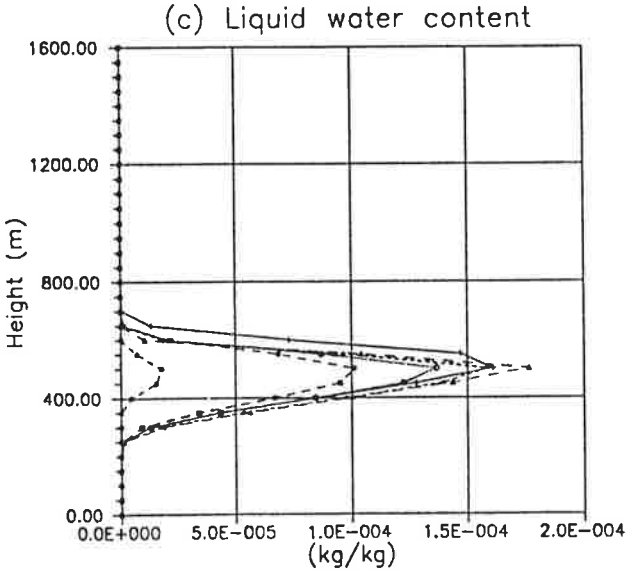
(c) Liquid water content
Height (m)
1600.00
1200.00
800.00
400.00
0.00
0.0E+000
5.0E-005
1.0E-004
1.5E-004
2.0E-004
(kg/kg)

Fig. 9

RUN 3

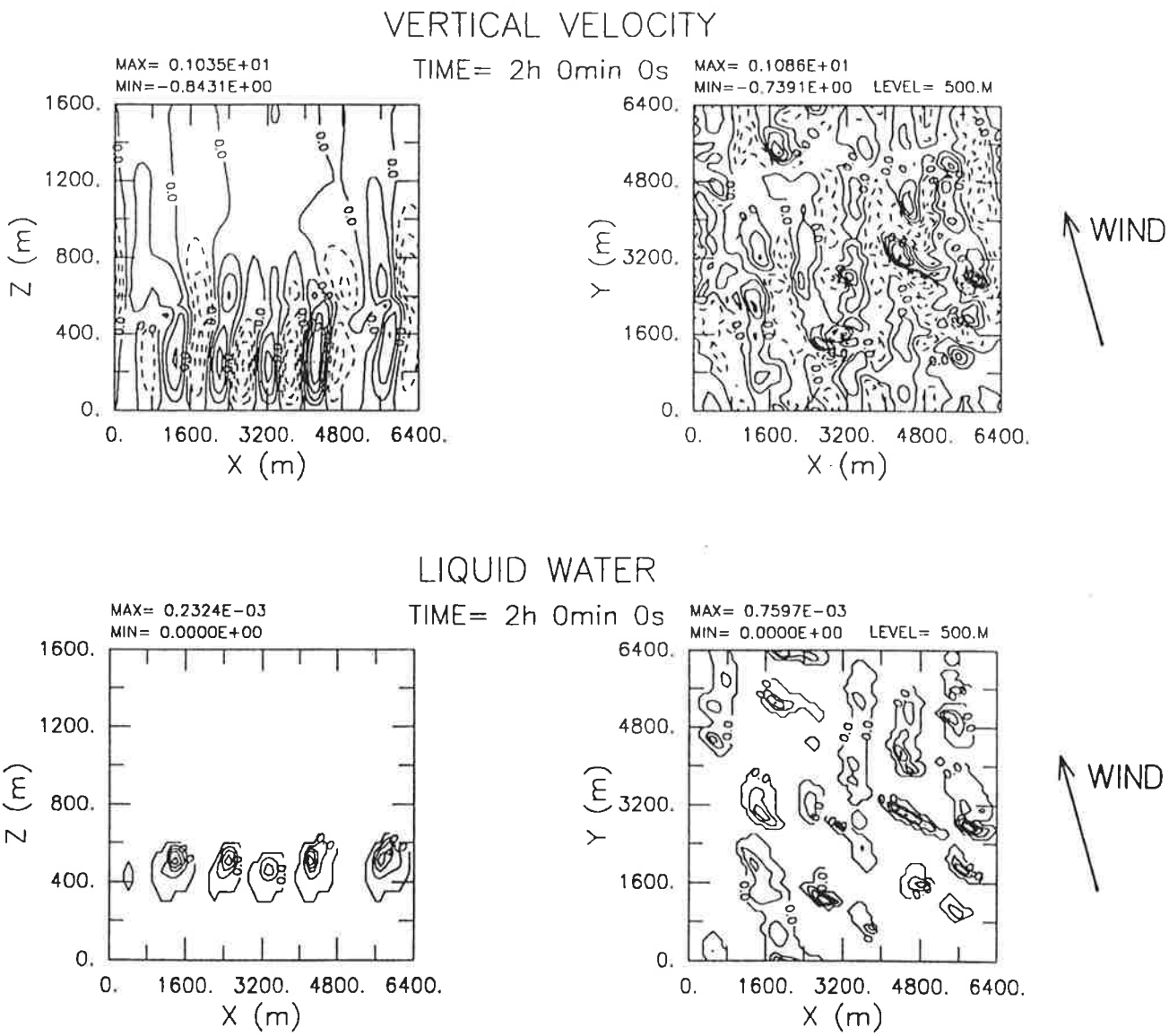
VERTICAL VELOCITY
MAX= 0.1035E+01
MIN=-0.8431E+00
TIME= 2h 0min 0s
MAX= 0.1086E+01
MIN=-0.7391E+00
LEVEL= 500.M
Z (m)
Y (m)
X (m)
0.
400.
800.
1200.
1600.
3200.
4800.
6400.
WIND
LIQUID WATER
MAX= 0.2324E-03
MIN= 0.0000E+00
TIME= 2h 0min 0s
MAX= 0.7597E-03
MIN= 0.0000E+00
LEVEL= 500.M
WIND

Fig. 10